The International Journal of Advanced Manufacturing Technology (2024) 130:2505–2522
https://doi.org/10.1007/s00170-023-12806-y

ORIGINAL ARTICLE

Volume energy density and laser power: key determinants in SLS-processed PA12 mechanical properties

Panagiotis Karmiris-Obratański[1,2] · Emmanouil L. Papazoglou[2] · Nikolaos E. Karkalos[2] · Angelos P. Markopoulos[2]

Received: 21 August 2023 / Accepted: 3 December 2023 / Published online: 18 December 2023

Abstract

Additive manufacturing (AM) represents a significant breakthrough in the field of engineering, revolutionizing the way products and components are designed and manufactured. Among the various methods used to employ polymer materials in AM, powder bed fusion (PBF) processes, specifically selective laser sintering (SLS), stand out as one of the most widely utilized approaches. This method offers substantial advantages over other AM techniques for treating polymers. However, SLS is inherently based on complex underlying physical mechanisms and phenomena and it involves a significant number of process parameters, making a comprehensive and extensive study of the process necessary. In the present article, we conduct an experimental study to examine the impact of two pivotal process parameters in SLS: volumetric energy density (VED) and nominal laser power (LP), on the mechanical properties of Polyamide 12 (PA12). The assessment of the material's mechanical behavior was conducted by measuring its tensile, compressive, and flexural properties, adhering to the respective ASTM standards. Additionally, we employed appropriate statistical tests, including the Coefficient of Variation (CV) to estimate the process's repeatability and consistency, and Fisher's least significant difference (LSD) method to determine significant differences between mean property values for different process parameters. The results revealed the impact of volumetric energy density (VED) and nominal laser power (LP) on each mechanical property and mechanical index. Furthermore, the study identifies general rules and trends related to the efficiency and feasible thresholds of the process. Finally, we provide an interpretation of the results based on the fundamental physical mechanisms, also supported by the respective XRD and microscopy images.

Keywords Powder bed fusion · Polyamide 12 · Mechanical properties · Volumetric energy density · Laser power · Material characterization

Nomenclature

$CAE_{0.3}$ (Kj)	Compressive absorbed energy at 0.3 strain
CME (MPa)	Compressive modulus of elasticity
CV	Coefficient of variation
CYS (MPa)	Compressive yield strength
FAE_{YP} (kJ)	Flexural absorbed energy at the yield point
FME (MPa)	Flexural MODULUS OF ELASTICITY
FYS (MPa)	Flexural yield strength
HS (mm)	Hatch space
LP (W)	Laser power
LSS (mm/s)	Laser scanning speed
PBT (mm)	Powder bed thickness
$TAE_{Fr.}$ (kJ)	Tensile absorbed energy until fracture
TFS (MPa)	Tensile fracture strength
TME (MPa)	Tensile modulus of elasticity
TUS (MPa)	Tensile ultimate strength
TYS (MP)	Tensile yield strength
VED (J/mm^3)	Volumetric energy density

✉ Panagiotis Karmiris-Obratański
karmiris@agh.edu.pl

[1] Department of Manufacturing Systems, Faculty of Mechanical Engineering and Robotics, AGH University of Krakow, 30-059 Kraków, Poland

[2] Laboratory of Manufacturing Technology, School of Mechanical Engineering, National Technical University of Athens, 157 80 Athens, Greece

1 Introduction

Selective laser sintering (SLS) is an additive manufacturing technique that employs principles from laser physics and powder material science to fabricate three-dimensional objects in a layer-by-layer manner [1, 2]. Powder bed fusion

(PBF) processes involve the selective fusion or melting of powdered material to create solid objects layer by layer. In these processes, particularly when treating polymer materials, CO_2 lasers are commonly utilized as high-energy–density sources that are directed onto the powder bed [3]. Upon exposure to the laser beam, the powdered material undergoes a rapid localized temperature increase [4]. The absorbed energy is converted into thermal energy, which induces either the melting or sintering of the polymer particles as they reach their melting point or glass transition temperature, respectively [5, 6]. Through diffusion and molecular bonding processes, the adjacent particles merged, creating a structurally integrated and solidified layer [7]. By optimizing various SLS process parameters, including laser power, scanning speed, and layer height, desired mechanical properties can be achieved. [8]. Additionally, preheating, powder bed, and sintering temperatures are fundamental for the proper densification and microstructure evolution during the process. According to German [9], all the aforementioned sintering parameters affect the complex thermodynamic stages of fusion and cooling [10–12]. In the context of optimizing SLS printing parameters, volumetric energy density (VED) emerges as an essential parameter, reflecting the amount of energy supplied to the powder bed by the laser per unit volume [13]. The VED can be considered as a valid and extreme important process index not only for the SLS process, but for the PBF processes in general, including the laser-PBF [14] or even the electron-beam-PBF process [15].

Compared to other additive manufacturing methods like FDM and SLA, SLS significantly reduces the need for support structures, especially when simple geometries have to be built as the un-sintered powder acts as a support structure [16]. Thus, there is significant saving both in time and material [17]. Semi-crystalline polymers, predominantly Nylon 12 and 11, have been demonstrated to sinter effectively, yielding superior mechanical characteristics compared to their amorphous polymer counterparts [18, 19]. Nonetheless, the occurrence of dimensional inaccuracies due to a volumetric contraction in the crystallization phase poses a considerable challenge [20]. As such, it is important for materials intended for SLS processing to have a melt temperature that significantly exceeds the crystallization temperature. This temperature difference ensures the retardation and reduction of crystallization during the fabrication process [21], enabling successive layers to form interlayer bonds within a more homogenous microstructural.

Recently, substantial effort has been directed towards determining the mechanism and mechanical characteristics of PA12 fabricated using the SLS technique. Li et al. [22] conducted an experimental study to identify the parameters essential for thermal modeling at component-scale during SLS of PA12. The results indicated that employing a convection coefficient value of 10 [W/m^2/°C] uniformly across all surfaces yields simulation outcomes most congruent with thermocouple readings. Additionally, based on their model they were able to predict with 89% accuracy the thermal history of the printed parts by using thermocouples to capture the thermal energy from the top surfaces. Using in-situ thermal and X-ray characterization, Hejmady et al. [23] investigated the time-dependent microstructure evolution during laser sintering of PA12. The results show significant differences in the microstructure due to the heat affected zone [23, 24]. As mentioned earlier, the VED serves as one approach to evaluate the influence of process parameters on mechanical characteristics. Using this method, Pereira et al. [25] examined the impact of laser scan spacing and powder layer thickness on the morphology and mechanical attributes of composite scaffolds produced via SLS. According to their findings, the powder bed thickness is the predominant factor affecting the mechanical properties of the scaffolds, followed by the laser scanning speed (LSS) [26, 27]. Wang et al. [28] investigated the VED's effect on the electrical properties of PA12 fabricated via SLS. The researchers found that utilizing a laser density of 0.03 [J/mm^2], resulted in optimal electrical properties, with a resistivity of up to 22 [GΩ·m]. Pilipovic et al. [29] investigated the influence of VED, the laser diameter and the hatch space on the mechanical properties. Their analysis revealed that the mechanical properties are intrinsically modulated by the laser energy density and the hatch space ratio. An increase in laser energy density was found to improve material strength. However, values exceeding 0.0667 [J/mm^2] had a negative effect, leading to material's overheating that results in component distortion, which in turn reduced tensile strength. Authors also emphasize the significance of the hatch space in relation to the laser beam diameter, which was referred as overlap ratio because it is directly correlated with the "actual" energy density (ED). Specifically, an overlap ratio greater than 1, where the hatch space is smaller than the laser beam diameter, results in areas of the powder bed being exposed to the laser beam more than once. Czelusniak and Amorim [30] investigated the impact of energy density on the mechanical properties of carbon fiber-reinforced PA12 composite parts produced through SLS. Utilizing a space-filling design, they found that maximum density is achieved at median energy densities, while increased part accuracy was associated with reduced energy densities. The printing accuracy surpassed 99.6%, maintaining this level of precision for energy densities less than 0.381 [J/mm^3]. In the Y-direction, accuracy consistently exceeded 98% for energy densities up to 0.212 [J/mm^3], but declined at higher energy densities. Conversely, the Z-direction exhibited the least robustness in terms of accuracy, with optimal values just above 95% at the lowest energy density, showing a systematic decrease with ascending energy densities [31]. Additionally, the findings suggest a trade-off between part accuracy and density, which is significantly

influenced by specific laser sintering settings. While maximum density is achieved at median energy densities, greater part accuracy is observed at reduced energy densities—a correlation that has been previously corroborated by Jansson and Pejryd [32].

Based on existing literature, mechanical properties constitute an area of research and study of significant interest, as they are directly related to the functionality of the fabricated end products. Numerous studies focus on the mechanical properties of specific types of components; for example, Geng et al. [33] investigated the mechanical properties of chiral auxetic stents produced using Selective Laser Sintering (SLS), while Yao et al. [34] characterized scaffolds that can be employed in bio related applications and fabricated with SLS in terms of their mechanical properties. Nevertheless, assessing mechanical properties in the field of AM poses challenges due to the complex relationship between the intrinsic material properties and the optimal processing parameters [35]; moreover, a high number of parameters significantly influence the process. Simultaneously, beyond the individual effects of each parameter, the combination of these process parameters also significantly influences the fabrication outcomes, thereby creating an even more complex system that needs an extensive study [36]. Finally, it is important to note that an ideal assessment of mechanical properties should encompass evaluations of tensile, compressive, and flexural characteristics of the material [37, 38]. This is because the behavior of a structural element varies significantly under different types of loading conditions. For instance, the likelihood of buckling or crushing under compressive stress is influenced by the slenderness of the structural element. Conversely, buckling is not an issue when the element experiences tensile stress. Bending stress, meanwhile, results from a combination of both compressive and tensile stresses, induced by internal moments. Therefore, a comprehensive analysis that includes tensile, compressive, and flexural properties can be deemed of substantial interest and value.

In accordance with the aforementioned discussion, the current study concentrates on the influence of process parameters on the post-SLS mechanical properties of materials. Specifically, the study provides a comprehensive analysis examining the interrelationship between VED and laser power in relation to tensile, compressive, and flexural properties. More specifically, our study rigorously evaluates these properties in accordance with ASTM standards. Within the scope of SLS 3D printing optimization, laser energy density and laser power are pivotal for accurate calibration. To this end, we conducted an in-depth investigation using varying VED levels (0.3, 0.5, 0.7, and 0.9 [J/mm^3]) along with Laser Power (LP) settings at 10 and 26 [W] to elucidate their combined influence on mechanical properties. PA12 powder, commonly used in SLS 3D printing, served as our material substrate for its distinct physicochemical characteristics. The study involved a rigorous evaluation of 120 samples to ensure robust and conclusive findings. The assessment of tensile, compressive, and flexural properties was based on several representative indices. Subsequent statistical analysis included the coefficient of variation (CV) to evaluate process repeatability and consistency was carried out, while Fisher's least significant difference (LSD) method was employed to discern significant variations in mean values across different process parameters. Additionally X-ray diffraction (XRD) and SEM microscopy were conducted to fundamentally interpret how volumetric energy density (VED) and laser power (LP) influence the physical properties of the polymeric material.

2 Materials and methods

In the present research, the impact of the SLS process parameters on the mechanical properties of PA12 was studied. More specifically, the aim was to define the effects of the VED and the combination of laser power—scanning speed on the tensile, flexural, and compression properties of the material after its processing with the SLS. Based on the relevant literature, there are a number of different definitions regarding the energy density. These include the linear energy density, the surface energy density, and the volumetric energy density, each of which has its own specific advantages and disadvantages [39]. In the current study the VED was chosen as index of the energy density as it is mathematically described by Eq. 1.

$$VED = \frac{LP}{LSS \bullet HS \bullet PBT} \tag{1}$$

with *VED* representing the Volumetric Energy Density in [W/mm^3], *LSS* representing the laser scanning speed in [mm/s], *HS* representing the Hatch Spacing in [mm], and *PBT* representing the Powder Bed Thickness in [mm].

To study the effect of different VEDs on the mechanical properties, four different levels of VED were applied. These levels were specifically set at 0.3, 0.5, 0.7, and 0.9 [J/mm^3]. For each VED level, a combination of low and high LP was utilized. Specifically, LP values of 10 and 26 [W] were used, along with the corresponding appropriate LSS (see Table 1).

PA12 powder was utilized in the production of specimens using the EOS c P100 SLS machine. The constant parameters used in the study were as follows: a build orientation angle of 0° (horizontal), a HS of 0.25 [mm], PBT of 0.1 [mm, and a beam offset of 0.15 [mm]. Following the printing process, all the specimens were stored in airtight plastic bags to prevent moisture absorption. PA12 is recognized as a versatile semi-crystal thermoplastic polymer material with favorable mechanical properties, including toughness,

Table 1 SLS process conditions

No	Laser Power [W]	Scan speed [mm/s]	VED [J/mm^3]	Constant parameters
1. (0.3L)	10	1333	0.3	Build orientation: angle of 0° (horizontal)
2. (0.5L)	10	800	0.5	
3. (0.7L)	10	571	0.7	
4. (0.9L)	10	444	0.9	Powder bed thickness: 0.1 [mm]
5. (0.3H)	26	3467	0.3	
6. (0.5H)	26	2080	0.5	Beam offset: 0.15 [mm]
7. (0.7H)	26	1486	0.7	
8. (0.9H)	26	1156	0.9	Hatch space: 0.25 [mm]

tensile strength, impact strength, and flexibility without fracture. Hence, it finds extensive application in additive manufacturing and has consequently acquired significant research attention.

The assessment of the mechanical properties involved conducting tensile, compression, and flexural tests in accordance with the corresponding ASTM Standards. More specifically, the tensile tests were carried out following the ASTM D638-14 standard under quasi-static conditions. The tests were performed using a nominal crosshead speed of 10 [mm/min], and given that the gauge length was 126 [mm] (on average) this value corresponds to a strain rate of $1.32 \times 10^{-3}[s^{-1}]$. From the stress–strain curves the tensile modulus of elasticity (TME), the tensile yield strength (TYS), the tensile ultimate strength (TUS), the tensile fracture stress (TFS), and the tensile absorbed energy until fracture ($TAE_{Fr.}$) were calculated. The compressive properties were determined by following the ASTM D695-15 standard with the nominal test speed set at 2 [mm/min] and the nominal deformation at 10 [mm]. From the stress–strain curves the compressive modulus of elasticity (CME), the compressive yield strength (CYS), and the compressive absorbed energy at the strain equal to 0.3 ($CAE_{0.3)}$ were calculated. Finally, the flexural properties were determined by following the ASTM D790-15 standard by conducting 3-point bending tests. The support span was set at 51 [mm] and the nominal crosshead speed at 2 [mm/min]. From the stress – strain curves the flexural modulus of elasticity (FME), the flexural yield strength (FYS), and the flexural absorbed energy at the yield point (FAE_{YP}) were calculated. Here it has to be clarified that for the tensile tests, the yield point corresponds to the end of the elastic region and the point of the maximum stress corresponds to the TUS. On the other hand, and based on the respective standards, the yield point in compression and bending corresponds to the maximum stress (thus there is no ultimate stress for compression and bending) and hence, in Sect. 3.5 aiming in a consistent and valid interpretation of the results the TUS, CYS, and FYS will be considered for comparison. All the mechanical tests were conducted on an Instron 4482 universal testing machine, and the results were processed by Bluehill software on a standard PC. The measurements were carried out at room temperature (25 °C) with low levels of humidity to avoid undesirable effects on the specimens. Lastly, to delve into the physical mechanisms that define the post-SLS mechanical properties, material characterization was conducted using SEM microscopy and XRD analysis. The XRD analysis was performed on a BRUKER D8 Advance Twin/Twin, and SEM images with a magnification of 500× were deemed most representative captured on a ThermoFisher SCIENTIFIC Phenom Desktop SEM.

The obtained results were analyzed using appropriate statistical tests. More specifically, according to the aforementioned ASTM standards, at least five specimens were tested for each condition. The CV, which is defined as the ratio of the standard deviation to the mean value, was calculated as an index of repeatability and consistency of the process. Additionally, Fisher's LSD method was employed to determine the significant differences between the mean values for the different process parameters [40].

3 Results and discussion

Semicrystalline thermoplastics like PA12 exhibit a heterogeneous, lamellar, and often spherulitic structure. Notably, several factors influence their deformation behavior, including the size, morphology, and perfection of spherulites, the strength of inter-spherulitic boundaries, and the physical structure of the crystalline phase [41]. At the same time, inherently, tensile, compression, and flexural tests have significant differences. Given that the plastic deformation of a material depends on the form of the applied stresses [42], it is reasonable to expect variations in the measured mechanical properties under different types of loads, such as tensile, compressive, and bending. For example, during the tensile tests, initially, upon elongation of the specimen, a uniform deformation is observed, as reflected by a consistent rise in load with increasing elongation. At a certain point, the specimen undergoes localized thinning, leading to the formation

of a neck. Subsequent elongation results in a reduction in load. The continued elongation primarily occurs by the progressive movement of the neck's shoulders along the length of the specimen, transitioning from its original cross section to a drawn cross section. Typically, the load reduction is continued until the fracture point is reached [42]. On the contrary, compressive testing typically involves the use of cylindrical samples. While the resulting stress–strain curve bears similarity to that of tensile tests, and the same consideration is given to the "toe region" as well as stress and strain definitions, compressive testing presents unique challenges. Specifically, issues such as buckling, barreling, and friction are encountered in compressive tests but not in tensile tests [43]. One additional example of why it is important to evaluate the mechanical properties in regard of the different load conditions is the crack propagation and the fracture behavior. Fracture refers to the formation of new surfaces through the creation and propagation of a crack within a material. In semicrystalline solids, the onset of cracks is typically preceded by "craze-like" features, which originate from void nucleation and subsequent growth. However, the specific fracture mechanism of a material is influenced by its resistance to plastic deformation. This resistance, in turn, is determined by factors such as segmental mobility, sample morphology, the local stress state, which significantly alters in the different testing, and the rate at which load is applied. Consequently, variations in fracture behavior can be anticipated across different mechanical tests, including tensile, compressive, and flexural evaluations [41]. Thus, considering the complexity of the fundamental mechanisms, coupled with the influence of process parameters on post-SLS material properties, it is both logical and anticipated that these parameters will have distinct effects on each mechanical property and index. To delve deeper into the relationships between process parameters and mechanical properties, techniques such as SEM and XRD will be employed to interpret and assess the outcomes of the mechanical tests.

3.1 Tensile Properties

In Table 2, the tensile mechanical properties are listed; while in Figs. 1, 2 and 3, the respective diagrams are presented.

In Fig. 1, the tensile modulus of elasticity vs. the VED, the tensile yield strength vs. the VED and the tensile ultimate strength vs. the VED are presented. From these plots, two main conclusions can be easily deduced: firstly, in general, the tensile properties increase for higher VEDs, and secondly, the employment of higher LS also results in higher tensile properties. More specifically, the TME increased approximately 79% and 59% between 0.3 and 0.9 [J/mm^3] VED for the 10 and 26 [W] LP, respectively.

Interestingly, the most significant increase in TME occurs as the VED increases from 0.3 to 0.5 [J/mm^3], with

Table 2 Tensile mechanical properties

#	TME [MPa]	CV of TME	TYS [MPa]	CV of TYS	TUS [MPa]	CV of TUS	TFS [MPa]	CV of TFS	$TAE_{Fr.}$ [kJ]	CV of TAE_{Fr}	Av. CV
0.3L	694.0	0.064	10.9	0.033	23.9	0.019	23.6	0.022	11.6	0.129	0.053
0.5L	1158.7	0.038	17.9	0.121	36.3	0.030	33.6	0.011	26.6	0.118	0.064
0.7L	1125.9	0.035	19.3	0.139	36.0	0.029	34.9	0.038	24.9	0.259	0.100
0.9L	1244.2	0.019	20.4	0.072	43.4	0.019	42.5	0.020	34.1	0.068	0.040
0.3H	839.0	0.037	12.4	0.099	28.9	0.013	28.3	0.016	21.9	0.090	0.051
0.5H	1243.7	0.009	24.0	0.040	40.9	0.011	32.8	0.012	40.6	0.058	0.026
0.7H	1193.4	0.016	24.3	0.072	37.8	0.006	29.8	0.015	37.3	0.086	0.039
0.9H	1330.7	0.055	24.4	0.094	43.0	0.031	36.8	0.038	40.0	0.135	0.071

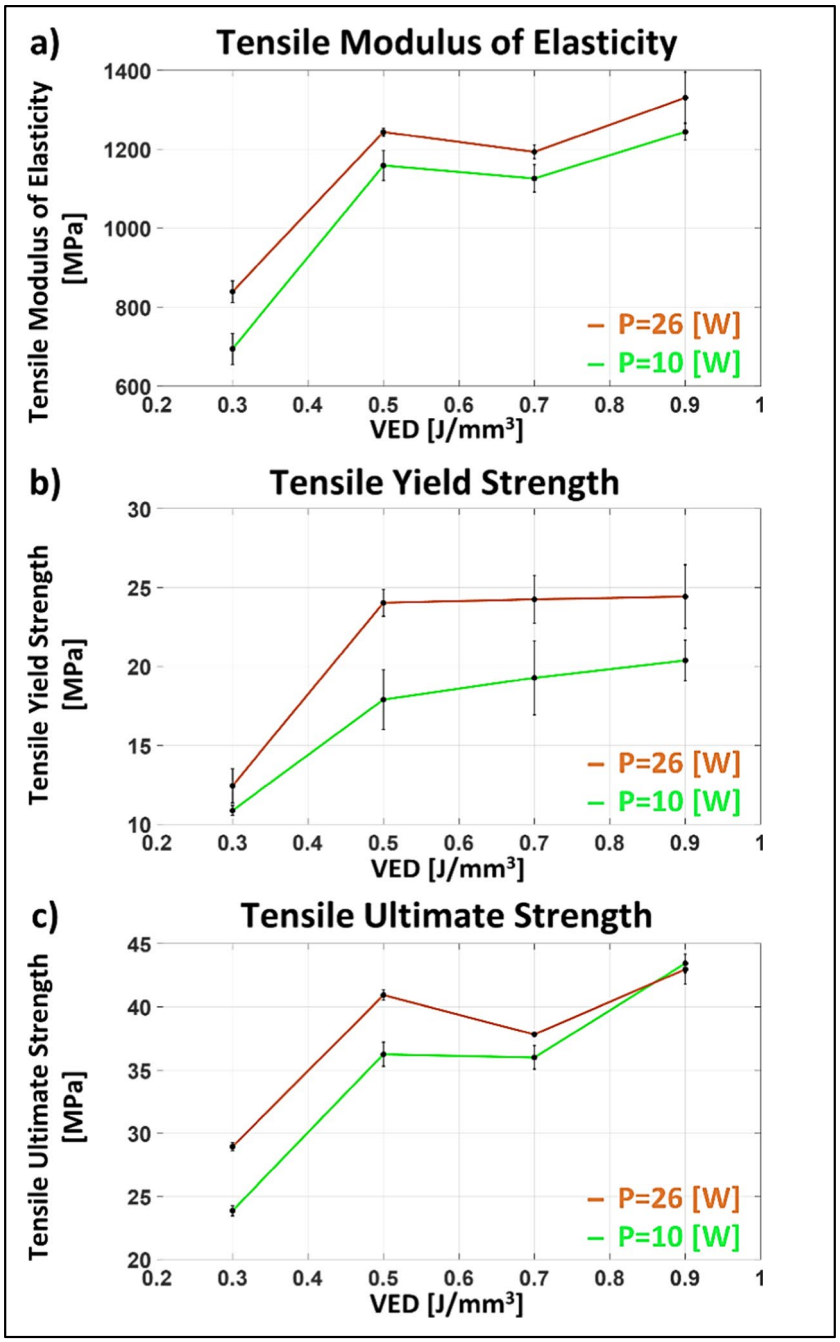

Fig. 1 **a** Tensile modulus of elasticity vs. VED, **b** tensile yield strength vs. VED, and **c** tensile ultimate strength vs. VED

an almost 70% and 48% increase for the 10 and 26 [W] LP, respectively. Despite the significant increase in TME as the VED increases, it is observed that for all the different process parameter combinations, the TME is still lower than that of the bulk material (approximately ≈1450 [MPa]), and only for the highest VED of 0.9 [J/mm^3] and the 26 [W] LP, the Young's modulus reaches a comparable value near 1400 [MPa]. The same patterns can be noted regarding the TYS, as the higher LP leads typically to higher TYS. Additionally, the increase in VED from 0.3 to 0.5 [J/mm^3] also results in a significant increase in TYS (approximately 64% for the 10 [W] LP and about 39.5% for the 26 [W] LP). However, it is noteworthy that further increases in VED beyond 0.5 [J/mm^3] does not result in any additional increase in TYS for both LPs. Finally, the TUS follows almost the same behavior as TME. Between 0.3 and 0.9 [J/mm^3] VED, the TUS increases by 81.5% for the 10 [W] LP and by 48.8% for the 26 [W] LP, with the most significant increase taking place between 0.3 and 0.5 [J/mm^3] VED.

In Fig. 2, a mapping of the statistically significant differences between the process parameters for the TME and the TUS based on the Fisher's LSD is presented. It can be

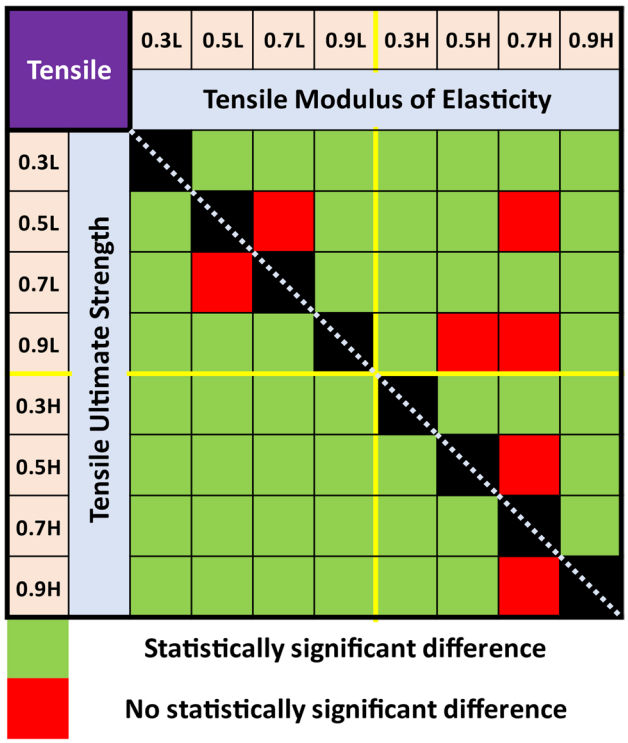

Fig. 2 The statistically significant differences between the process parameters for the TME and the TUS based on the Fisher's LSD test

deduced that, as a general conclusion, the different VEDs and the combination of process parameters have a significant impact on both TME and TUS as statistically significant differences are observed for most combinations of different process parameters. The only parameter that seems to "overlap" with the others regarding TME is the 0.7 [J/mm^3] VED with 26 [W] LP (0.7H), which does not have a statistically significant difference with three other parameter combinations (i.e., 0.5L, 0.9L, and 0.5H).

With a combined assessment of the results for TME, TYS, and TUS, it can be concluded that the major increase in these properties occurs as the VED increases from 0.3 to 0.5 [J/mm^3], while further increases in VED result in only slight increases in TME and TUS. Furthermore, considering that the TYS does not change for VEDs higher than 0.5 [J/mm^3], it can be inferred that as the VED increases, the material becomes stiffer (higher TME), but its elastic region is relatively decreased since the TYS shows less increase compared with the TME or even remains constant despite the increase in TME. Regarding TUS, it is evident that higher VEDs typically result in higher TUS, a property that is related to the material's limits before failure. To fully assess the total material strength, the TFS and the $TAE_{Fr.}$ have to be also considered. From the respective diagrams of Fig. 3, it is evident that higher VEDs result in higher TFS for the 10 [W] LP with an increase of almost 80% between 0.3 and 0.9 [J/mm^3] VED. Interestingly for VEDs higher than 0.5 [J/mm^3], the utilization of 26 [W] LP leads to lower TFS values for the same VED. At first sight, this behavior seems quite peculiar since it is observed only for the TFS, as for all the previous tensile properties, the higher LP for the same VED typically results in a higher property value. Nevertheless, considering the physical meaning of the TFS, there is a reasonable interpretation for the result. Based on a typical stress–strain curve for polymers, the stress decreases gradually after reaching the TUS, particularly as the material enters the necking region, until the point of fracture is reached [44]. Given this gradual decrease in stress, an increased capability for plastic deformation during necking would imply a lower TFS. Therefore, TFS should not be evaluated as an isolated index but should be correlated with other tensile property indices. Lower TFS values at higher LP levels can be explained by the improved printing quality achieved at a 26 [W] LP, allowing the material to undergo greater plastic deformation before collapsing completely and thus lower TFS is recorded. Conversely, the extremely low TFS value for the 10 [W] LP and the 0.3 [J/mm^3] VED may be attributed to the overall low tensile properties resulting from this combination of process parameters, which in turn leads to a correspondingly low TFS. Finally, the increase in TFS at higher VED levels when a 10 [W] LP is employed could be attributed to an improvement in the ultimate load-carrying properties, as evidenced by the TYS and TUS values. However, this may not suggest an enhanced capability for extensive plastic deformation; rather, it could point to a limited necking area. This interpretation is further supported by the results for both the TUS and the $TAE_{Fr.}$. The conclusion regarding the impact of the VED and the process combinations on the $TAE_{Fr.}$ is quite clear, with increase in VED between 0.3 and 0.5 [J/mm^3] resulting in a significantly higher $TAE_{Fr.}$ and also, with the use of higher LP for the same VED leading to higher $TAE_{Fr.}$. This is a reasonable and expected outcome since, in practice, $TAE_{Fr.}$ mainly depends on all the previous tensile indexes, thus, it can be considered as an overall summarization index of the material strength. As a noteworthy comment, it seems again that the 0.7 [J/mm^3] is not favorable and/or superior, indicating that this particular VED is somehow "peculiar" regarding the material's obtained tensile properties.

Finally, it has to be mentioned that all the CV values are relatively low, with most of them being less than 0.1, indicating an acceptable repeatability of the process. The lowest average CV value for the tensile properties (0.026) is calculated for VED 0.5 [J/mm^3] with the utilization of 26 [W] LP, while the highest (0.1) is observed for VED 0.7 [J/mm^3] with the utilization of 10 [W] LP. For all the VEDs except 0.9 [J/mm^3], the use of higher LP results in a lower average CV. However, and as an overall conclusion regarding the repeatability and consistency of the process with

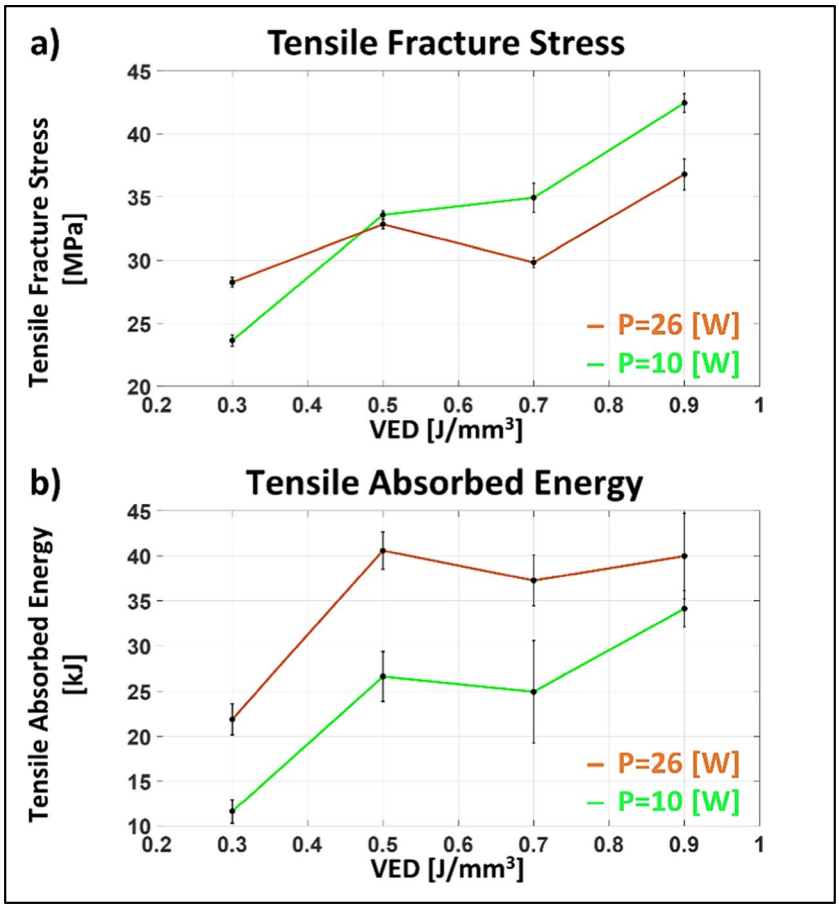

Fig. 3 **a** Tensile fracture stress vs. VED and **b** tensile absorbed energy vs. VED

respect to the tensile properties, it can be deduced that the process for these specific parameters shows a high consistency with low CV values compared with values from the relevant literature [45].

3.2 Compressive properties

In Table 3, the compressive mechanical properties are listed; while in Fig. 4, the respective diagrams are presented.

From the data in Table 3 and the respective plots in Fig. 4, it is evident and reasonable to deduce that the VED has a significant impact on the material's compressive properties. More specifically, for the 10 [W] and the 26 [W] LP, the increase in VED from 0.3 to 0.7 [J/mm^3] leads to approximately 90% and 67% higher CME respectively. Interestingly, the further increase of VED up to 0.9 [J/mm^3], results in only a slight increase of CME for the 10 [W] LP and no statistically significant increase for the 26 [W] LP (see Fig. 5). It has to be noticed that the bulk material's average CME which is approximately ≈1600 [MPa], is significantly higher than all the measured CME values of the SLS processed material, indicating that the SLS process results a sintered material of lower compressive properties. It is also interesting, that based on Fig. 5, a number of different process

Table 3 Compressive mechanical properties

#	CME [MPa]	CV of CME	CYS [MPa]	CV of CYS	$CAE_{0.3}$[kJ]	CV of $CAE_{0.3}$	Av. CV
0.3L	415.5	0.099	31.9	0.057	29.9	0.030	0.062
0.5L	467.4	0.087	39.7	0.031	36.8	0.031	0.050
0.7L	788.4	0.046	37.0	0.007	42.7	0.014	0.022
0.9L	889.8	0.113	46.6	0.051	53.7	0.063	0.076
0.3H	581.3	0.104	32.1	0.088	37.5	0.056	0.083
0.5H	871.7	0.185	40.5	0.034	45.7	0.037	0.085
0.7H	972.0	0.094	43.0	0.004	48.3	0.038	0.045
0.9H	909.9	0.044	47.1	0.016	59.4	0.038	0.033

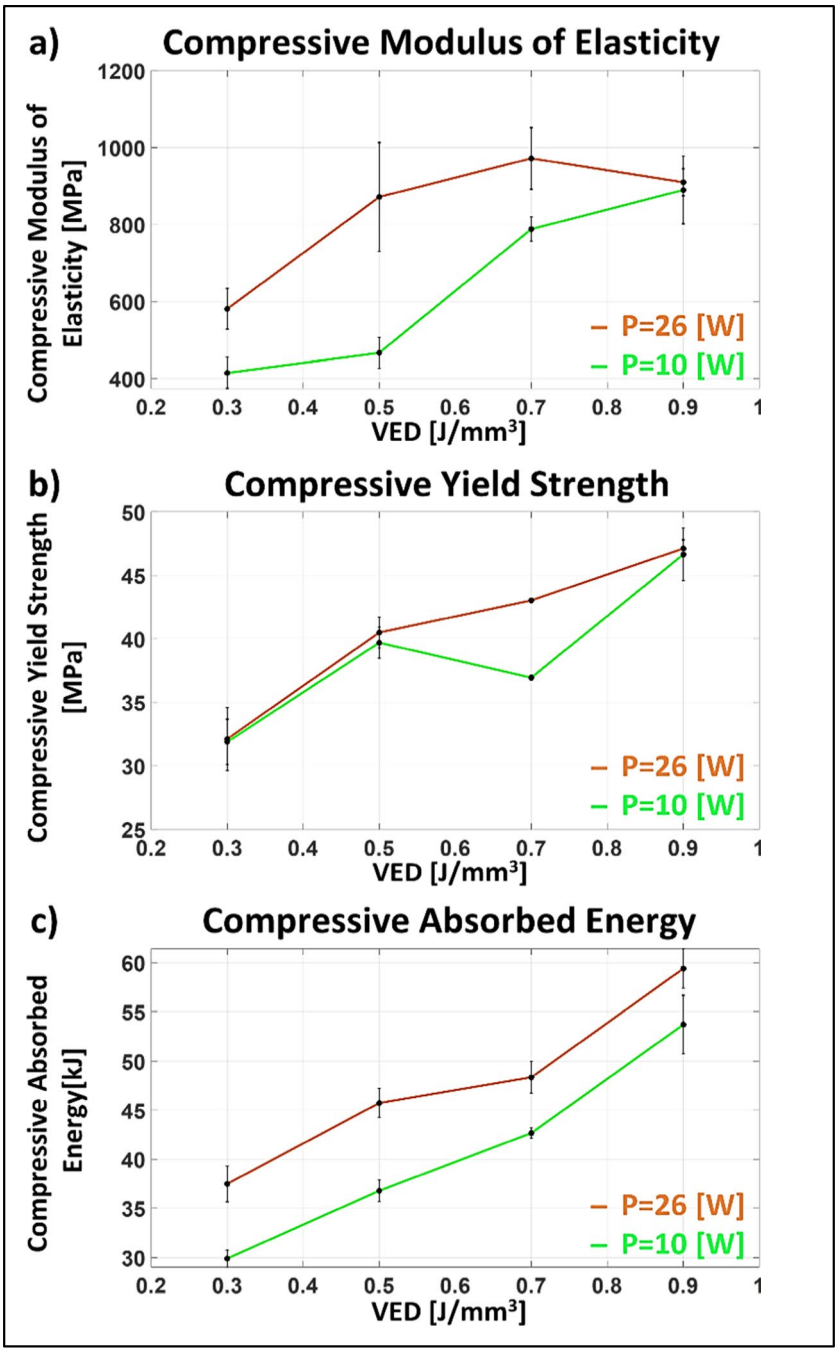

Fig. 4 **a** Compressive modulus of elasticity vs. VED, **b** compressive yield strength vs. VED, and **c** compressive absorbed energy at strain 0.3 vs. VED

parameters combinations, in practice, yield similar results regarding the CME since there is no statistically significant difference between the measures CME values.

Concerning the impact of the process parameters on the CYS, based on the results of Fig. 4 b and Fig. 5, it is deduced that the VED primarily and significantly affects the CYS, while the LP has rather a minor impact since for 0.3, 0.5, and 0.9 [J/mm^3] VED the CYS is the same for both LPs. The CYS increases approximately 46% as the VED increases from 0.3 to 0.9 [J/mm^3]. Nevertheless, again these values are lower than the typical CYS of the bulk material (≈75 [MPa]). Based on Fig. 4 c, an almost linear relation between the $CAE_{0.3}$ and the VED is evident, with the $CAE_{0.3}$ increasing almost 80% as the VED increases from 0.3 to 0.9 [J/mm^3]. The impact of the employed LP is minor, since, based on the conducted Fisher's LSD test, for the same VED, only for 0.7 [J/mm^3], there is a statistically significant difference for the $CAE_{0.3}$ between the 10 and 26 [W] LP. Finally, the calculated CV values indicate that the process falls within acceptable limits of repeatability and consistency regarding the compressive properties, with all the average CV values being less than 0.1. However, it is interesting to note

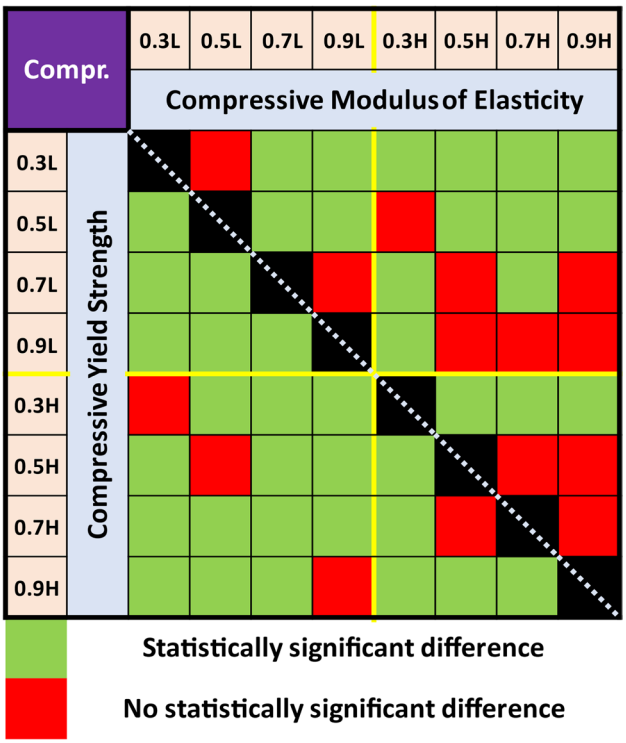

Fig. 5 The statistically significant differences between the process parameters for the CME and the CYS based on the Fisher's LSD test

that the CME is a more sensitive index, as it shows higher CV values compared to the CV values for the CYS and the $CAE_{0.3}$which are noticeably low.

3.3 Flexural properties

In Table 4, the flexural mechanical properties are listed; while in Fig. 6, the respective diagrams are presented. The flexural properties of PA12 after the SLS process are expected to gather increased scientific interest because, inherently during bending, the specimens are subjected to a more complex mechanical testing mode. This complexity arises from the presence of regions experiencing tensile stress and regions experiencing compressive stress simultaneously.

From the diagrams of Fig. 6, the previously mentioned interesting behavior of the material concerning its flexural properties after the SLS process is evident. Firstly, based on Fig. 6 a and Fig. 7, it is deduced that the FME is either the same or lower when the 26 [W] LP is used compared to when the 10 [W] LP is utilized. Notably, the general outcome regarding the tensile and compressive properties was that, as a rule of thumb, higher LP leads to higher or the same mechanical properties, since only for the TFS the lower LP resulted in higher TFS values. This general trend does not seem to be applied for the flexural properties. Additionally, it is also apparent that for the 26 [W] LP, all the different VEDs result in the same FME, indicating that for the 26 [W] LP, the VED does not have a statistically significant impact on the FME. In practice, only the increase of VED from 0.3 to 0.5 [J/mm^3] for the 10 [W] LP resulted in a statistically significant impact on the FME, as it was increased by approximately 52%. However, after this, for further increase of VED, there was no actual change in FME values. Again, the FME of the material after the SLS process is lower than the respective of the bulk material ((≈ 1700 [MPa]) indicating that the SLS resulted in lower flexural elasticity. The FYS follows similar trends as the FME with lower LP generally leading to higher or the same FYS. However, unlike FME, the FYS is significantly affected by changes in VED for both LPs. It is interesting to note that the increase in VED does not necessarily result in higher FYS, as seen in the change between 0.3 and 0.5 [J/mm^3] where, for the high LP, the FYS is decreased. Nevertheless, in general, higher VED leads to higher FYS, with an approximately 57% increase in FYS as the VED changes from 0.3 to 0.9 [J/mm^3] for the 10 [W] LP. Finally, the FAE_{YP} exhibits a behavior similar to the FYS, with the VED highly impact the FAE_{YP}. An increase in VED results in an increase in the FAE_{YP} (increase over 170% of the FAE_{YP} as the VED increases from 0.3 to 0.9 [J/mm^3]). On the other hand, only for the 0.5 [J/mm^3] VED there is a statistically significant difference between the low and the high LP, indicating

Table 4 Flexural mechanical properties

#	FME [MPa]	CV of FME	FYS [MPa]	CV of FYS	FAE_{YP} [kJ]	CV of FAE_{YP}	Av. CV
0.3L	709.6	0.062	36.6	0.085	0.4	0.178	0.108
0.5L	1076.7	0.068	52.4	0.009	0.8	0.070	0.049
0.7L	1064.8	0.085	50.5	0.079	0.8	0.091	0.085
0.9L	1070.6	0.078	57.6	0.047	1.1	0.067	0.064
0.3H	833.7	0.071	37.7	0.064	0.5	0.028	0.054
0.5H	811.1	0.318	30.8	0.129	0.4	0.171	0.206
0.7H	846.8	0.145	45.2	0.055	0.8	0.122	0.107
0.9H	759.5	0.178	47.8	0.101	1.1	0.094	0.124

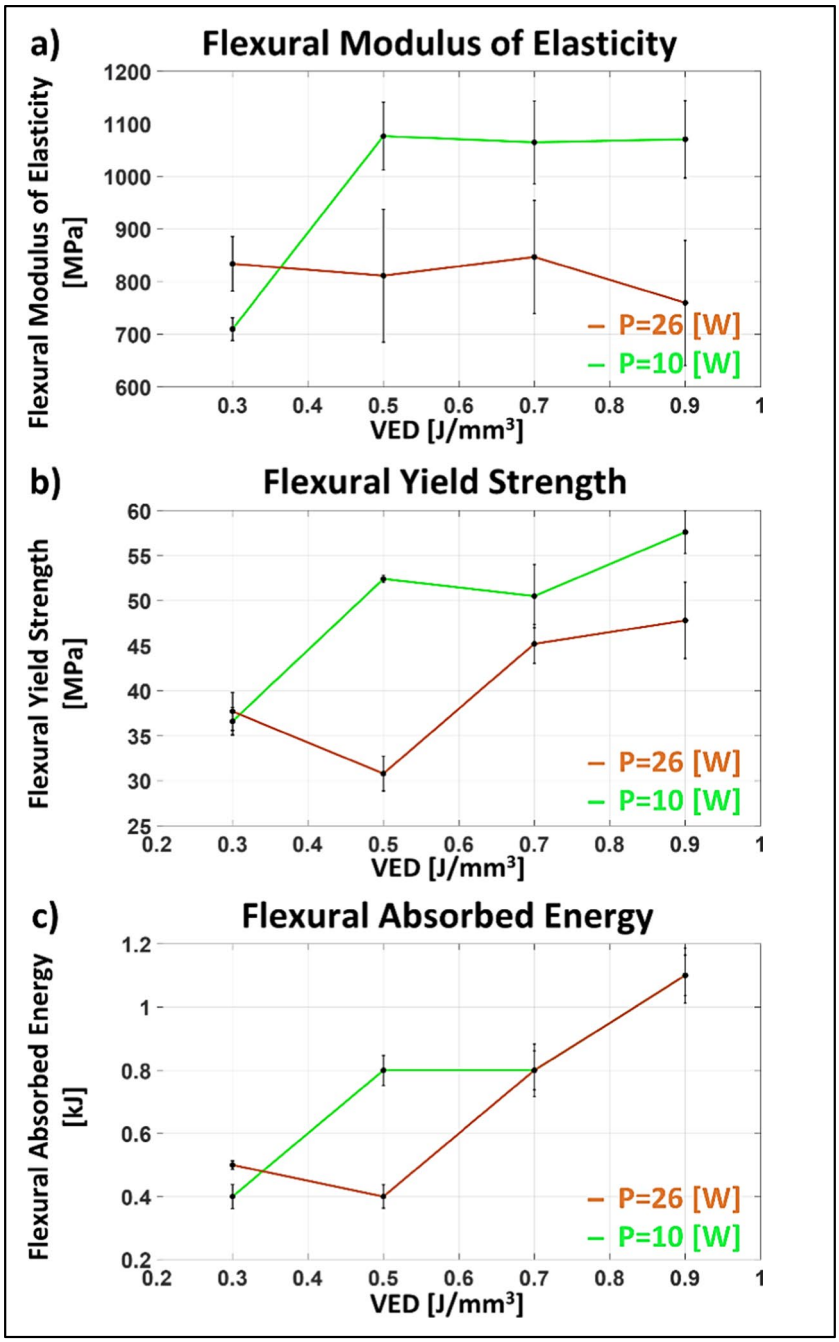

Fig. 6 **a** Flexural modulus of elasticity vs. VED, **b** flexural yield strength vs. VED, and **c** flexural absorbed energy at the yield point vs. VED

that the VED is the dominant parameter regarding the FAE_{YP} while the LP does not seem to significantly affect the FAE_{YP}. Concerning the repeatability and consistency of the process regarding the material's flexural properties, based on the CV values, it is concluded that the process falls within acceptable limits, although higher CV values are calculated compared to those of the tensile and compressive properties. The CVs when the higher LP was employed for 0.5, 0.7, and 0.9 [J/mm^3] VEDs are significantly higher than those of the low LP, indicating that the higher utilized LP results in a material with less consistent flexural properties. Interestingly, the highest average CV value is calculated for the 0.5 [J/mm^3] VED and 26 [W] LP, a process parameter combination which also exhibits the highest average CV for the compressive properties but the lowest average CV for the tensile properties. This strongly indicates that the material's mechanical properties after SLS have to be evaluated and assessed comprehensively, taking into consideration all the main material properties like tensile, compressive, and flexural, rather than focusing on just one of them.

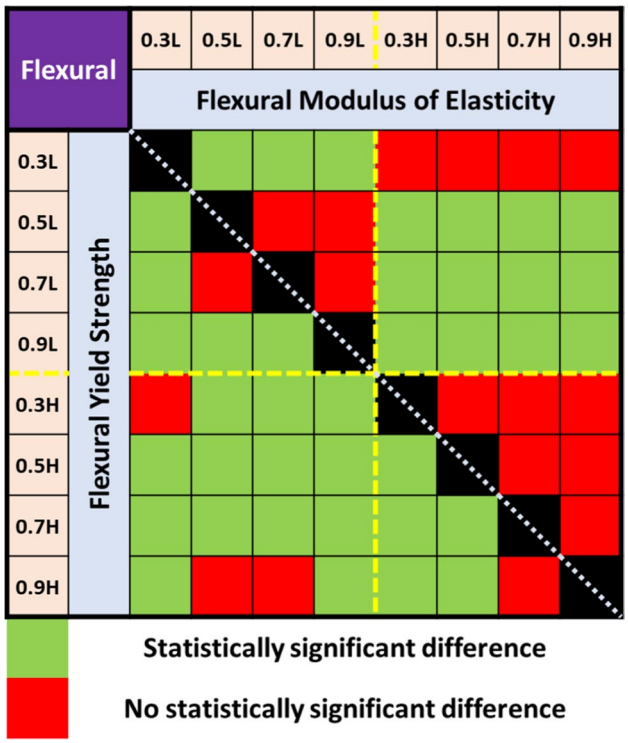

Fig. 7 The statistically significant differences between the process parameters for the FME and the FYS based on the Fisher's LSD test

3.4 Material characterization

In Fig. 8, SEM images from the fracture zone of the tensile test specimens are presented for various combinations of VED and Laser LP, indicating the impact of these parameters. For a VED of 0.3 [J/mm^3] and an LP of 10 [W] (as shown in Fig. 8a), increased porosity is evident, along with the presence of partially melted and poorly bonded material. Numerous spheroid-like particles are observed, which may indicate incomplete sintering and melting processes. This increased porosity and material discontinuity could explain the compromised material properties observed under these process parameters; specifically, the material exhibits low coherence, and the porosity serves as sites for crack initiation and propagation. When the VED is maintained at 0.3 [J/mm^3] but the LP is increased to 26 [W] (Fig. 8b), there is a noticeable reduction in spheroid-like particles, and the material exhibits improved coherence. However, significant porosity remains, as evidenced by the presence of numerous voids and cracks. Increasing the VED to 0.9 [J/mm^3] while maintaining a low LP of 10 [W] (as depicted in Fig. 8c) yields a more homogeneous material that appears to be fully and adequately melted and bonded. However, the presence of cracks and voids persists. The improved material quality at higher VEDs accounts for enhanced material properties, while the presence of material discontinuities suggests that lower LP settings are suboptimal for the process. When the VED is set to 0.9 [J/mm^3] and combined with a higher LP of 26 [W], the material becomes substantially more homogeneous with limited porosity. This suggests that the increased power and energy levels are sufficient for complete material melting. Some voids may be attributed to gas release, either entrapped in the molten material or resulting from PA12 degradation due to localized temperature increases. The overall material homogeneity and coherence justify the superior mechanical properties observed at higher VED and LP settings.

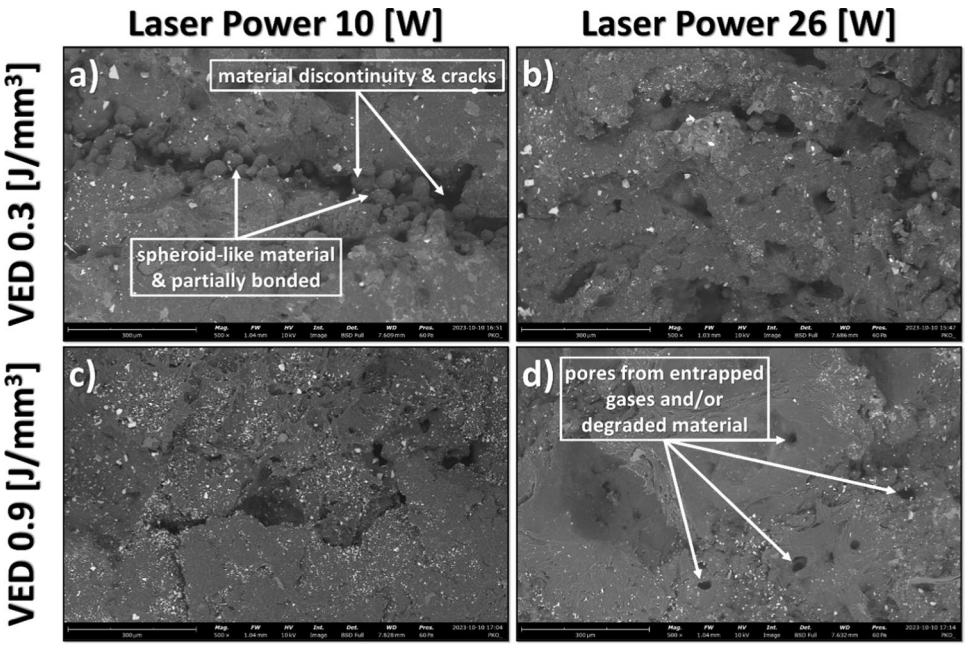

Fig. 8 SEM images × 500 for **a** VED 0.3 [J/mm^3] and LP 10 [W], **b** VED 0.3 [J/mm^3] and LP 26 [W], **c** VED 0.9 [J/mm^3] and LP 10 [W], and **d** VED 0.9 [J/mm.^{3}] and LP 10 [W]

In Fig. 9, the crystallinity percentage for the different VEDs and LPs presented, while Fig. 10 presents the corresponding XRD plots for **a** 10 [W] LP and **b** 26 [W] LP. Within the plots of Fig. 10, the characteristic peaks of the PA12 γ phase, observed around 11° and 21° 2Theta, are evident [46]. The crystallinity percentage is calculated as the ratio of the area corresponding to crystalline phases to the total area, considering a 2Theta degree range from 6 to 35. A count greater than $7.5 \bullet 10^3$ was taken as indicative of a crystalline phase. Firstly, Fig. 9 indicates that a higher LP consistently results in an increased crystallinity percentage for a specific VED. This trend might explain the generally enhanced mechanical properties observed when the higher LP was utilized. Crystallinity is inherently complex, heavily influenced by the material's thermal history, which is directly governed by the processing parameters. Typically,

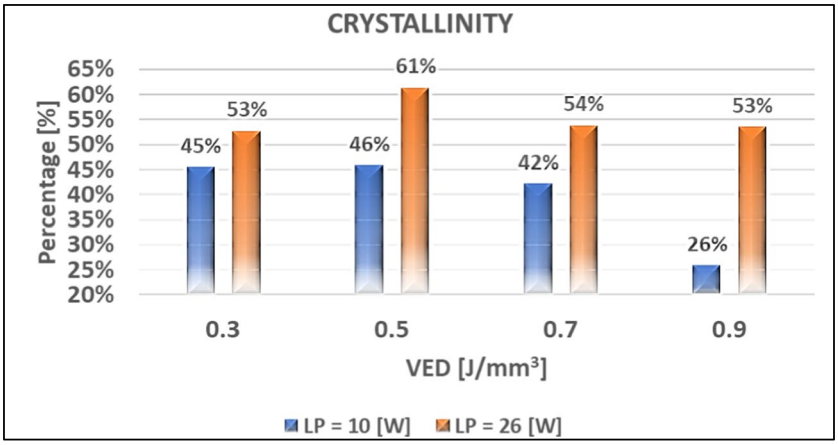

Fig. 9 Crystallinity percentage depending on the VED and the LP

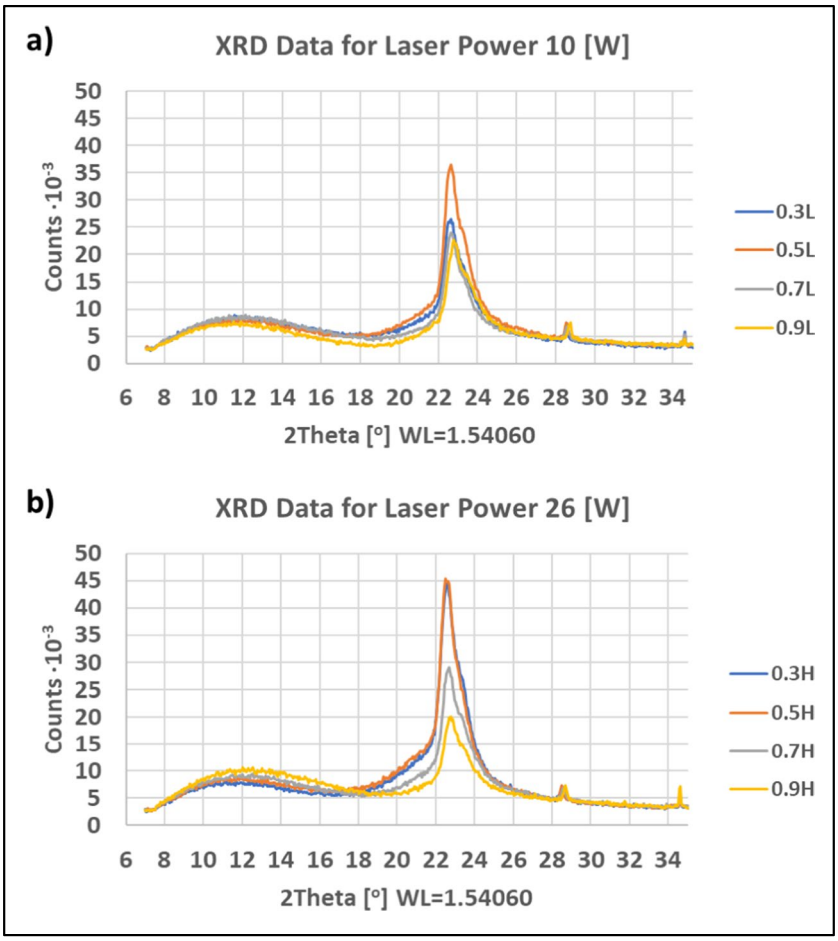

Fig. 10 XRD plots depending the VED for **a** LP = 10 [W] and **b** LP = 26 [W]

greater crystallinity correlates with increased Young's modulus and tensile strength. In contrast, elongation at break often diminishes with heightened crystallinity [47]. These basic correlations offer insights into the elevated mechanical properties noted for the 26 [W] LP. Furthermore, they shed light on why certain metrics, such as TFS, FME, and FYS, register higher values for the lower LP, given the reduced elongation at the break point. Interestingly, for both LPs, the highest crystallinity was observed at the 0.5 [J/mm^3] VED, which corresponds to the threshold VED where a significant improvement in tensile properties was noted. This peak in crystallinity could explain the notably rise in tensile properties observed between 0.3 and 0.5 [J/mm^3] VED.

However, it is essential to emphasize that the degree of crystallinity is just one factor influencing the overall mechanical properties. The quality of sintering/melting and the resultant bonding are other pivotal aspects. Despite the 0.9 [J/mm^3] VED exhibiting lower or comparable crystallinity compared to the lower VEDs, it typically leads to enhanced mechanical properties. Considering the SEM images in Fig. 8, this can reasonably be attributed to superior sintering and melting processes, resulting in a more uniform material without voids or discontinuities, thus yielding superior mechanical properties. The higher VED and the respective thermal fields might induce a reduced degree of crystallinity and potential degradation. However, the additional energy and the aforementioned improved sintering process likely compensates for any property losses stemming from reduced crystallinity.

3.5 Discussion

Based on the obtained results of the tensile, compressive, and flexural properties of PA12 after the SLS process, a general and overall assessment of the conclusions can be made. It is evident that the VED is a process parameter of major significance, while the LP also plays a pivotal role for some properties. The VED is directly related to the available energy responsible for the melting and sintering of the material, ultimately converting the powder into bulk material. Practically, there exists an "window" of acceptable VED levels [35, 48]. The lower VED threshold is primarily dictated by the minimum power and energy required for successful melting and sintering, whereas the upper limit is constrained by the risk of material overheating and polymer degradation. However, it is important to note that the definition of VED also encompasses several constant parameters that could independently affect these conclusions. Therefore, the use of the VED index should be exercised with caution in the study and optimization of the process. According to the specific definition of VED (Eq. 1), it is deduced that the minimum threshold for acceptable mechanical properties is 0.5 [J/mm^3]. This is because increasing the VED from 0.3 to 0.5 [J/mm^3] resulted in significant improvements in nearly all material properties. While further increases in VED can also enhance certain properties, it can be reasonably concluded that, under these specific constant conditions (i.e., HS and PBT), the lower limit of VED is 0.5 [J/mm^3].

In more details, the physical interpretation of these conclusions is that for lower VEDs the available energy is not sufficient for the optimal and ideal melting and/or sintering of the powder. As a result, weaker interparticle and interlayer bonding occur, leading to lower density and ultimately inferior mechanical properties [25]. Suboptimal process parameters and inadequate fusion may consequently lead to the formation of voids and the existence of loose particles, both of which can negatively affect the material's behavior and result in inferior mechanical properties [49–51]. Thus, when the VED threshold is reached, the mechanical properties are significantly improved, as a high degree of sintering and solidification is achieved. At the same time, pores and other defects that may act as local stress concentrators are also reduced, further enhancing the material's strength [47]. The non-consistent improvement of the mechanical properties for higher VEDs can be explained by considering that when the highest density (or almost the highest) is attained for a specific VED, further increases in VED cannot significantly improve the material's density and, consequently, its mechanical properties [50]. In fact, excessive increases in VED will eventually lead to extensive material degradation, resulting in subsequent material burn, pore formation, and destruction of favorable microstructure [52]. This can reasonably explain at a fundamental level why, for certain indexes, the increase in VED not only does not result in improved properties but, on the contrary, leads to inferior properties. However, in a comprehensive evaluation of the results, the degree of crystallinity should be taken into account. The crystallinity degree peaks at 0.5 [J/mm^3] VED for both LPs, and a decline is noted for higher VEDs. Nonetheless, the beneficial impact of increased available energy on material coherence overbalances the reduction in crystallinity, leading to a post-SLS material that generally exhibits enhanced mechanical properties. The LP, in practice, corresponds to the energy input rate to the system, which, in the case of constant VED, also affects the nominal LSS. The energy rate that the powder material can efficiently handle depends on the material's thermophysical properties (i.e., density, specific heat, and thermal conductivity), with the energy rate falling within ranges optimal for forming melting and sintering temperature profiles. In other words, the LP must be sufficient to heat the material to its melting point, but it is limited by the possibility of rapid localized heating and the degradation of the material. Additionally, the higher power results in higher LSS, and thus, shorter exposure times, which directly affects

the kinematics of the sintering process [51]. Based on the obtained results, the 26 [W] LP does not seem to have any general negative effect on the material's properties, and hence, it can be deduced that the 26 [W] nominal LP can be considered as a feasible nominal LP for the SLS process of PA12 for VEDs in the range of 0.3 to 0.9 [J/mm^3]. Nevertheless, the fact that for the higher VEDs (i.e., 0.7 and 0.9 [J/mm^3]) the improvement in material's mechanical properties shows some reduction, especially for the 26 [W] LP, indicates that the upper limits of the efficient and optimal VEDs and LP are close to the upper limits of the current DoE setup.

Finally, in Fig. 11, the maximum Modulus of Elasticity and the maximum Stress for each of the three mechanical testing modes are presented. These two indexes were chosen since the measurements are reduced to the area of the specimen, and thus, a valid comparison can be done. An initial observation is that the maximum TME and TME are resulted from the same process parameters combination, namely, 0.9 [J/mm^3] VED and 26 [W] LP, while the optimal FME is achieved at 0.5 [J/mm^3] VED and 10 [W] LP. However, the 0.9 [J/mm^3] VED and 26 [W] LP appears more consistent across all three mechanical properties, as indicated by the greater symmetry of the blue triangle compared to the orange in Fig. 11 a. Interestingly, the maximum tensile and flexural stress values were observed when using 0.9 [J/mm^3] VED and 10 [W] LP, whereas the peak compressive stress was recorded at 0.9 [J/mm^3] VED and 26 [W] LP. However, upon a critical evaluation of the results (see Tables 2, 3, and 4, and Fig. 11b), it becomes evident that, in practice, the 0.9 [J/mm^3] VED for both LP values yielded comparable, if not nearly the same, maximum tensile and flexural stresses. As such, the combination of 0.9 [J/mm^3] VED with 26 [W] LP emerges as the most favorable printing choice, presenting the most balanced and uniform mechanical properties across all standard loading types. As a concluding observation, analysis shows that, on average, the TME across all different process parameter combinations is 34% greater than the CME and 16% greater than the FME. Conversely, the TUS averages 11% below the CYS and 26% below the FYS. This observation further underscores the importance of not solely assessing mechanical properties under tensile loading but also giving due consideration to compressive and flexural properties.

To provide a comprehensive conclusion to this article, it is important to highlight the limitations of the present study and offer directions for potential future work. Firstly, as previously noted, the term VED, by definition encompasses several process parameters, including, but not limited to, LP and LSS, specifically, the HS and the PBT. For the purposes of this study, and to maintain a manageable DOE, these parameters were held constant. While this choice presents a necessary limitation of the research, these variables do directly impact the process and thus represent a significant area for future investigation due to their practical and scientific implications. Moreover, in line with established standards, all properties were gauged under standard environmental conditions. However, given the characteristics of polymeric materials, exploring factors such as humidity absorption and temperature, particularly in terms of their effects on post-SLS mechanical properties, would be enlightening. Such research could bridge the current gap between laboratory-based, standard-driven mechanical property definitions and the actual performance of a printed component in real-world scenarios. Lastly, a promising direction for further research would involve developing models and meta-models to study and predict post-SLS material properties based on the selected process parameters. Such a methodology could streamline the optimization of the process by reducing the need for extensive experimental work. In addition, through comprehensive modeling and simulation, invaluable insights into the processes and underlying physical mechanisms can be achieved.

4 Conclusions

In the current study, an experimental investigation of the mechanical properties of the PA12 after SLS was carried out. The main control parameters were the VED and the LP. More specifically, to study the effect of different VEDs on the mechanical properties, four different levels of VED were applied (0.3, 0.5, 0.7, and 0.9 [J/mm^3]); while for each VED level, a combination of low and high LP (10 and 26 [W]) was utilized. The materials mechanical properties were assessed

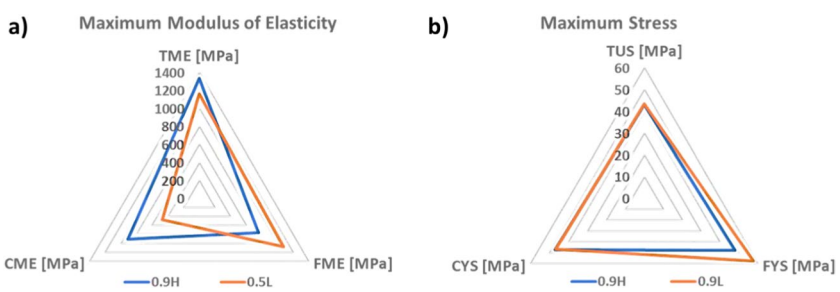

Fig. 11 **a** Maximum modulus of elasticity and **b** maximum stress for the three mechanical testing modes

in respect of the tensile, compressive and flexural properties by following the respective ASTM standards. For the tensile properties, the tensile modulus of elasticity, the tensile yield strength, the tensile ultimate strength, the tensile fracture strength, and the tensile absorbed energy until fracture were calculated. From the compressive stress – strain diagrams the Compressive modulus of elasticity, the compressive yield strength, and the compressive absorbed energy at 0.3 strain were calculated, while the flexural properties were estimated based on the flexural modulus of elasticity, the flexural yield strength, and the flexural absorbed energy at the yield point. Finally, the experimental results were analyzed using appropriate statistical tests, including the coefficient of variation to assess repeatability and consistency of the process and Fisher's least significant difference method to determine significant differences between mean values for different process parameters. The main deduced conclusions can be summarized as:

- The tensile properties are directly and highly affected by the VED, with an increase in VED typically resulting in an increase in the tensile modulus of elasticity, tensile ultimate strength, and tensile fracture strength. However, the tensile yield strength and the tensile absorbed energy until fracture only increase up to 0.5 [J/mm^3] VED, while higher VEDs do not lead to statistically significant change of these properties. The LP has a clear impact on the material's behavior under tensile stress, as higher LP generally results in superior tensile properties.
- The VED also has a significant impact on the material's compressive properties. The Compressive Modulus of Elasticity increases with an increase in VED up to 0.7 [J/mm^3], but the higher VED of 0.9 [J/mm^3] does not result in a further increase. As for the compressive yield strength and the compressive absorbed energy at 0.3 strain, higher VED values typically lead to higher values. The LP also appears to have a significant impact on the compressive modulus of elasticity and the compressive absorbed energy at 0.3 strain.
- The flexural properties exhibit the most peculiar behavior. the flexural modulus of elasticity showed a noticeable increase only for 0.5 [J/mm3] VED and 10 [W] LP; while, on the other hand, the flexural yield strength and the flexural absorbed energy until the yield point increased for higher VEDs. Interestingly, the LP has a minor impact on the material's flexural behavior, as higher LP leads to inferior or the same flexural properties.
- As a more general conclusion, it is deduced that the lower threshold for the material to obtain some acceptable mechanical properties is the 0.5 [J/mm^3] VED, while further increases in VED lead to a "diminished" improvement of the material's characteristics. The 26 [W] LP falls within the range of acceptable LPs without causing any significant degradation or deterioration of the material's properties due to rapid and excessive heating, when it is combined with the appropriate laser speed values. Finally, in general, the repeatability and consistency of the process fall within acceptable limits with significantly low CV values, especially for specific process parameter combinations.
- An increase in LP results in less amount of unsintered and unmelted material. However, it does not effectively limit porosity and material coherence. The rise in VED is the primary factor that leads to a more homogeneous material with fewer voids and discontinuities.
- Regarding crystallinity, the peak crystallinity percentage was recorded for 0.5 [J/mm^3] VED. An increase beyond this VED value leads to a reduction in the crystallinity percentage. Moreover, a higher LP consistently results in an elevated crystallinity percentage for a given VED. Crucially, the enhancement in material properties, owing to improved material coherence and bonding at higher VEDs, offsets any decline brought about by reduced crystallinity.

Declarations

Ethical approval This article does not contain any studies with human participants or animals performed by any of the authors.

Informed consent Not applicable.

Conflict of interest The authors declare no competing interests.

References

1. Monkova K, Monka P (2017) Qualitative parameters of complex part produced by additive approach. In: 2017 8th International Conference on Mechanical and Aerospace Engineering (ICMAE). IEEE, pp 691–694
2. Allahham N, Fina F, Marcuta C et al (2020) Selective laser sintering 3D printing of orally disintegrating printlets containing

ondansetron. Pharmaceutics 12:1–13. https://doi.org/10.3390/pharmaceutics12020110
3. Westphal E, Seitz H (2021) A machine learning method for defect detection and visualization in selective laser sintering based on convolutional neural networks. Addit Manuf 41:101965. https://doi.org/10.1016/j.addma.2021.101965
4. Drummer D, Rietzel D, Kühnlein F (2010) Development of a characterization approach for the sintering behavior of new thermoplastics for selective laser sintering. Phys Procedia 5:533–542. https://doi.org/10.1016/j.phpro.2010.08.081
5. Jain PK, Pandey PM, Rao PVM (2009) Effect of delay time on part strength in selective laser sintering. Int J Adv Manuf Technol 43:117–126. https://doi.org/10.1007/s00170-008-1682-3
6. Ling Z, Wu J, Wang X et al (2019) Experimental study on the variance of mechanical properties of polyamide 6 during multi-layer sintering process in selective laser sintering. Int J Adv Manuf Technol 101:1227–1234. https://doi.org/10.1007/s00170-018-3004-8
7. Dadbakhsh S, Verbelen L, Verkinderen O et al (2017) Effect of PA12 powder reuse on coalescence behaviour and microstructure of SLS parts. Eur Polym J 92:250–262. https://doi.org/10.1016/j.eurpolymj.2017.05.014
8. Yao B, Li Z, Zhu F (2020) Effect of powder recycling on anisotropic tensile properties of selective laser sintered PA2200 polyamide. Eur Polym J 141:110093. https://doi.org/10.1016/j.eurpolymj.2020.110093
9. German RM (2014) Sintering: from empirical observations to scientific principles. Elsevier
10. Zarringhalam H, Hopkinson N, Kamperman NF, de Vlieger JJ (2006) Effects of processing on microstructure and properties of SLS Nylon 12. Mater Sci Eng A 435–436:172–180. https://doi.org/10.1016/j.msea.2006.07.084
11. Gibson I, Shi D (1997) Material properties and fabrication parameters in selective laser sintering process. Rapid Prototyp J 3:129–136. https://doi.org/10.1108/13552549710191836
12. Charoo NA, Barakh Ali SF, Mohamed EM et al (2020) Selective laser sintering 3D printing – an overview of the technology and pharmaceutical applications. Drug Dev Ind Pharm 46:869–877. https://doi.org/10.1080/03639045.2020.1764027
13. Scipioni Bertoli U, Wolfer AJ, Matthews MJ et al (2017) On the limitations of volumetric energy density as a design parameter for selective laser melting. Mater Des 113:331–340. https://doi.org/10.1016/j.matdes.2016.10.037
14 Antunes LHM, Hoyos JJ, Andrade TC et al (2021) Deformation-induced martensitic transformation in Co-28Cr-6Mo alloy produced by laser powder bed fusion: comparison surface vs bulk. Addit Manuf 46:102100. https://doi.org/10.1016/j.addma.2021.102100
15. Li B, Wang L, Wang B et al (2022) Electron beam freeform fabrication of NiTi shape memory alloys: crystallography, martensitic transformation, and functional response. Mater Sci Eng A 843:143135. https://doi.org/10.1016/j.msea.2022.143135
16. Calignano F (2014) Design optimization of supports for overhanging structures in aluminum and titanium alloys by selective laser melting. Mater Des 64:203–213. https://doi.org/10.1016/j.matdes.2014.07.043
17. Han W, Kong L, Xu M (2022) Advances in selective laser sintering of polymers. Int J Extrem Manuf 4:. https://doi.org/10.1088/2631-7990/ac9096
18. de Leon AC, Chen Q, Palaganas NB et al (2016) High performance polymer nanocomposites for additive manufacturing applications. React Funct Polym 103:141–155. https://doi.org/10.1016/j.reactfunctpolym.2016.04.010
19. Venoor V, Park JH, Kazmer DO, Sobkowicz MJ (2021) Understanding the effect of water in polyamides: a review. Polym Rev 61:598–645. https://doi.org/10.1080/15583724.2020.1855196
20. Benedetti L, Brulé B, Decreamer N et al (2019) Shrinkage behaviour of semi-crystalline polymers in laser sintering: PEKK and PA12. Mater Des 181:107906. https://doi.org/10.1016/j.matdes.2019.107906
21. Hou Y, Gao M, An R et al (2023) Surface modification of oriented glass fibers for improving the mechanical properties and flame retardancy of polyamide 12 composites printed by powder bed fusion. Addit Manuf 62:103195. https://doi.org/10.1016/j.addma.2022.103195
22. Li C, Snarr SE, Denlinger ER et al (2021) Experimental parameter identification for part-scale thermal modeling of selective laser sintering of PA12. Addit Manuf 48:102362. https://doi.org/10.1016/j.addma.2021.102362
23. Hejmady P, van Breemen LCA, Hermida-Merino D et al (2022) Laser sintering of PA12 particles studied by in-situ optical, thermal and X-ray characterization. Addit Manuf 52:102624. https://doi.org/10.1016/j.addma.2022.102624
24. Tian X, Peng G, Yan M et al (2018) Process prediction of selective laser sintering based on heat transfer analysis for polyamide composite powders. Int J Heat Mass Transf 120:379–386. https://doi.org/10.1016/j.ijheatmasstransfer.2017.12.045
25. Pereira TF, Silva MAC, Oliveira MF et al (2012) Effect of process parameters on the properties of selective laser sintered Poly(3-hydroxybutyrate) scaffolds for bone tissue engineering. Virtual Phys Prototyp 7:275–285. https://doi.org/10.1080/17452759.2012.738551
26. Hou Y, Wang W, Bartolo P (2022) Application of additively manufactured 3D scaffolds for bone cancer treatment: a review. Bio-Design Manuf 5:556–579. https://doi.org/10.1007/s42242-022-00182-7
27. Wegner A (2021) Introduction to powder bed fusion of polymers. In: Additive Manufacturing. Elsevier, pp 33–75
28. Wang Z, Li H, Wang J et al (2021) Influence of laser energy density and printing angle on the electrical properties of PA12 made by SLS. IEEE Trans Dielectr Electr Insul 28:906–914. https://doi.org/10.1109/TDEI.2021.009503
29. Pilipović A, Brajlih T, Drstvenšek I (2018) Influence of processing parameters on tensile properties of SLS polymer product. Polymers (Basel) 10:1208. https://doi.org/10.3390/polym10111208
30. Czelusniak T, Amorim FL (2020) Influence of energy density on selective laser sintering of carbon fiber-reinforced PA12. Int J Adv Manuf Technol 111:2361–2376. https://doi.org/10.1007/s00170-020-06261-2
31. Stoia DI, Marşavina L, Linul E (2019) Correlations between process parameters and outcome properties of laser-sintered polyamide. Polymers (Basel) 11:1850. https://doi.org/10.3390/polym11111850
32. Jansson A, Pejryd L (2016) Characterisation of carbon fibre-reinforced polyamide manufactured by selective laser sintering. Addit Manuf 9:7–13. https://doi.org/10.1016/j.addma.2015.12.003
33. Geng LC, Ruan XL, Wu WW et al (2019) Mechanical properties of selective laser sintering (sls) additive manufactured chiral auxetic cylindrical stent. Exp Mech 59:913–925. https://doi.org/10.1007/s11340-019-00489-0
34. Yao D, Zhao Z, Wu Z et al (2023) Characterization of PA12/HA composite scaffolds based on selective laser sintering. J Mech Behav Biomed Mater 145:106000. https://doi.org/10.1016/j.jmbbm.2023.106000
35. Vande Ryse R, Edeleva M, Van Stichel O et al (2022) Setting the optimal laser power for sustainable powder bed fusion processing of elastomeric polyesters: a combined experimental and theoretical study. Materials (Basel) 15:385. https://doi.org/10.3390/ma15010385
36. Razaviye MK, Tafti RA, Khajehmohammadi M (2022) An investigation on mechanical properties of PA12 parts produced by a SLS

3D printer: an experimental approach. CIRP J Manuf Sci Technol 38:760–768. https://doi.org/10.1016/j.cirpj.2022.06.016
37. Marsavina L, Stoia DI (2020) Flexural properties of selectively sintered polyamide and Alumide. Mater Des Process Commun 2:1–5. https://doi.org/10.1002/mdp2.112
38. Cobian L, Rueda-Ruiz M, Fernandez-Blazquez JP et al (2022) Micromechanical characterization of the material response in a PA12-SLS fabricated lattice structure and its correlation with bulk behavior. Polym Test 110:107556. https://doi.org/10.1016/j.polymertesting.2022.107556
39. Wischeropp TM (2021) Advancement of selective laser melting by laser beam shaping. Springer
40. Frey B (2022) The SAGE Encyclopedia of Research Design, 2nd ed. SAGE Publications Ltd
41. Kausch HH, Plummer CJG (2001) Semicrystalline polymers: Fracture Properties. Encyclopedia of Materials: Science and Technology. Elsevier, München, pp 8420–8427
42. Ward IM, Sweeney J (2012) Mechanical properties of solid polymers. Wiley
43. Reed PE (1999) Mechanical properties and testing of polymers. Springer, Netherlands, Dordrecht
44. Lim H, Hoag SW (2013) Plasticizer effects on physical–mechanical properties of solvent Cast Soluplus® Films. AAPS PharmSciTech 14:903–910. https://doi.org/10.1208/s12249-013-9971-z
45. Baba MN (2022) Flatwise to upright build orientations under three-point bending test of nylon 12 (PA12) Additively. 12:. https://doi.org/10.3390/polym14051026
46. Kuracina R, Szabová Z, Buranská E et al (2021) Determination of fire parameters of polyamide 12 powder for additive technologies. Polymers (Basel) 13:2–11. https://doi.org/10.3390/polym13173014
47. Pavan M, Faes M, Strobbe D et al (2017) On the influence of inter-layer time and energy density on selected critical-to-quality properties of PA12 parts produced via laser sintering. Polym Test 61:386–395. https://doi.org/10.1016/j.polymertesting.2017.05.027
48. Lupone F, Padovano E, Pietroluongo M et al (2021) Optimization of selective laser sintering process conditions using stable sintering region approach. Express Polym Lett 15:177–192. https://doi.org/10.3144/expresspolymlett.2021.16
49. Bourell D, Wohlert M, Harlan N et al (2002) Powder densification maps in selective laser sintering. Adv Eng Mater 4:663–669. https://doi.org/10.1002/1527-2648(20020916)4:9%3c663::AID-ADEM663%3e3.0.CO;2-1
50. Caulfield B, McHugh PE, Lohfeld S (2007) Dependence of mechanical properties of polyamide components on build parameters in the SLS process. J Mater Process Technol 182:477–488. https://doi.org/10.1016/j.jmatprotec.2006.09.007
51. Beal VE, Paggi RA, Salmoria GV, Lago A (2009) Statistical evaluation of laser energy density effect on mechanical properties of polyamide parts manufactured by selective laser sintering. J Appl Polym Sci 113:2910–2919. https://doi.org/10.1002/app.30329
52. Peyre P, Rouchausse Y, Defauchy D, Régnier G (2015) Experimental and numerical analysis of the selective laser sintering (SLS) of PA12 and PEKK semi-crystalline polymers. J Mater Process Technol 225:326–336. https://doi.org/10.1016/j.jmatprotec.2015.04.030